Electronic Supporting Information

A Ternary Fe(II)-terpyridyl Complex-based Single Platform for Reversible Multiple-ion Recognition

Alok Kumar Singh[a],*, Gajanan Pandey[a], Kaman Singh[a], Abhinav Kumar[b],
Manoj Trivedi[c], Vikram Singh[d],*

[a]Department of Applied Chemistry, Babasaheb Bhimrao Ambedkar University, Lucknow, India

[b]Department of Chemistry, University of Lucknow, Lucknow

[c]Department of Chemistry, University of Delhi, Delhi

[d]Centre for Nanoscience and Nanotechnology, Panjab University, Chandigarh, India

*E-mail:aloksinghchemistry@gmail.com; vsingh@pu.ac.in

Materials and Methods. Most of the metals salts used in sensing studies were purchased from BDH chemicals Ltd, Sigma Aldrich and used as received. 2-Acetyl pyridine, pyridine-4-carboxaldehyde, $FeCl_2$ and NH_4PF_6 were purchased from Sigma Aldrich and store in N_2 atmosphere. Deuterated solvents were purchased from Sigma Aldrich and stored at 4 °C. Ethanol and acetonitrile (HPLC grade) were purchased from Merck and distilled before use using reported methods.[S1] Double distilled water was used whenever required.

Fluorescence spectroscopy experiments were performed on Varian Cary eclipse fluorescence instrument (slit width, 5 nm) with a quartz cuvette (path length, 1cm). UV-vis-NIR spectra were recorded using Ananalytik Jena SPECORD 250 with a quartz cuvette (path length = 1cm, volume = 3 ml). ATR-IRIR spectra were recorded on Perkin-Elmer spectrophotometer in range 750-4000 cm^{-1} equipped with ZnSe crystal. ^{1}H-NMR spectrum at room temperature were recorded on Jeol JNMECX 400P spectrometer using either CD_3CN or DMSO-d_6. All chemical shifts (δ) were recorded in ppm with reference to tetramethylsilane (TMS). The pH of the solution was fixed with EUTECH Instruments pH 510, calibrated with buffer solutions of pH 4.00 and 9.00 before each measurement.
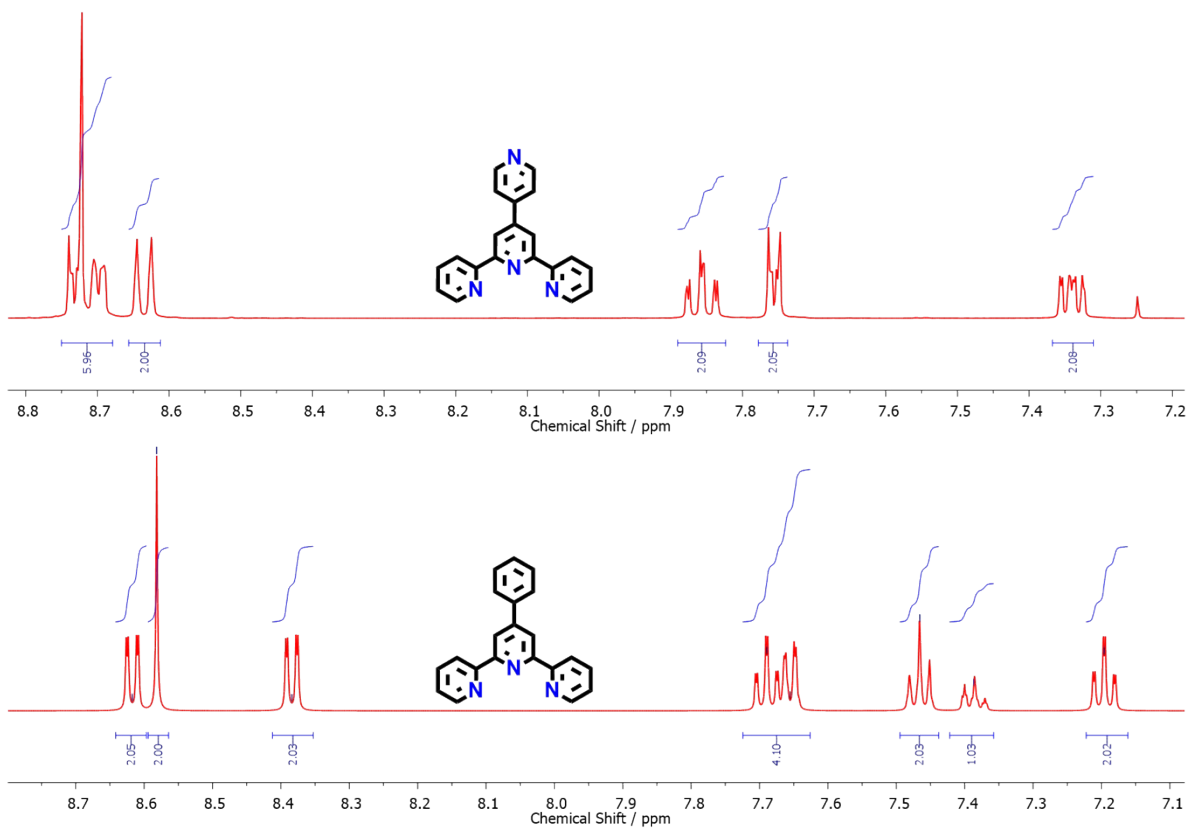
Synthesis of 4'-pyridyl-2,2':6',2''-terpyridine (PT) and 4'-phenyl-2,2':6',2''-terpyridine (PhT). These ligands were prepared according to reported procedures resulting in white needle shaped crystals and characterized using ^{1}H NMR (**figure S1**).[S2, S3]

Synthesis of 1. PT (78 mg, 0.25mmol) was dissolved in 20 mL of hot ethanol and then $FeCl_2$ (31.9 mg, 0.25 mmol) in 10 mL ethanol was added dropwise with constant stirring under a N_2 atmosphere and the reaction mixture was stirred for 20 min. Then **PhT** (77.9 mg, 0.25mmol) in 20 mL ethanol was added drop wise with constant stirring. Subsequently, the reaction-mixture was refluxed with stirring for 7 h. After cooling to room temperature, the reaction-mixture was filtered and subsequently, **1** was precipitated out by the addition of saturated ethanolic solution of NH_4PF_6 and collected by vacuum filtration. The residue was washed with ample amount of water followed by diethyl ether, dried under vacuum and recrystallized using a mixture of acetonitrile and acetone to get the micro-crystalline solid. Yield: 52%. See **figure S1** for ^{1}H NMR of **PT** and **PhT** and **figure S2** for ^{1}H NMR of **1** (400 MHz, DMSO-d_6) δ/ppm: 9.22 (d, 2H, J = 3.37 Hz, H$^{3'}$), 9.19 (d, 2H, J = 3.82 Hz, H$^{3'a}$), 9.02 (d, 2H, J = 7.5 Hz, H^m), 8.62 (m, 4H, H^3+H^{3a}), 8.32 (d, 2H, J = 8.2 Hz, H^o), 8.23 (t, 2H, J = 7.6 Hz, H^{ma}), 7.94 (m, 4H, H^4+H^{4a}), 7.81

(t, 2H, J = 7.86 Hz, H^{oa}), 7.73 (m, 1H, H^p), 7.19 (dt, 4H, J= 7.8, 4.6 & 1.6 Hz, H^6+H^{6a}), 7.09 (dt, 4H, J = 7.2, 5.0 & 1.8 Hz, H^5+H^{5a}). See **figure S3** for ^1H-^1H COSY spectrum of **1**. See **figure S4** for ESI-MS (+ve mode): m/z 361 corresponding to $((M-2PF_6)/2) + Na^+$. See **figure S5a** for UV-vis (10^{-5} M, CH_3CN) λ_{max}/nm ($\varepsilon/10^3$ dm^3 mol^{-1} cm^{-1}): 567 (25.9). See **figure S5b** for ATR-IR (ZnSe): 1608 (*w*), 1410 (*w*), 833 (*vs*). Elemental analysis: (calculated) C: 51.00; H: 3.03; N: 10.16 (observed) C: 50.10; H: 3.13; N: 9.86.

Preparation of ppm-level solutions of metal salts. A stock solution of 1000 ppm of various salts of KCN, KF, KOH, KNO_3, NH_4PF_6, KNO_2, KSCN, CH_3COONa, K_2SO_4, $NaClO_4$, $KHCO_3$, KI, KBr, KCl, K_2CO_3, $AgNO_3$, $FeCl_3$, $FeCl_2$, $LiNO_3$, $NiCl_2.6H_2O$, $MnCl_2.4H_2O$, $CuCl_2.2H_2O$, $CoCl_2.6H_2O$, $Pb(NO_3)_2$, $FeSO_4.7H_2O$ and $Hg(NO_3)_2.H_2O$ were made by dissolving 10 mg of each salts in 10 ml of suitable solvents:- water for aqueous medium and mixture of dry solvents *i.e.,* acetonitrile/ethanol/DMSO for non-aqueous medium. These solutions were used for sensing and recovery experiments. For proof-of-concept experiments, pool and tap water samples were collected and filtered before preparing stock solution (1000 ppm) of CN^-/F^-/OH^-.

Detection procedure for CN^-, F^- and OH^-: A 2 ml solution of **1** (10^{-5} M, CH_3CN/tris-HCl buffer; pH = 7.0) was treated with 2 µL stock solution of CN^-/F^-/OH^- in water (~1.0 ppm), which mixed well within seconds. Continuous addition of the respective analyte (2 µL aliquot) to **1** was monitored using UV-vis and emission spectroscopy at room temperature. ^1H NMR in DMSO-d_6 and ATR-IR analyses at room temperature was conducted after mixing required equivalents of **1** and the particular anion solution.

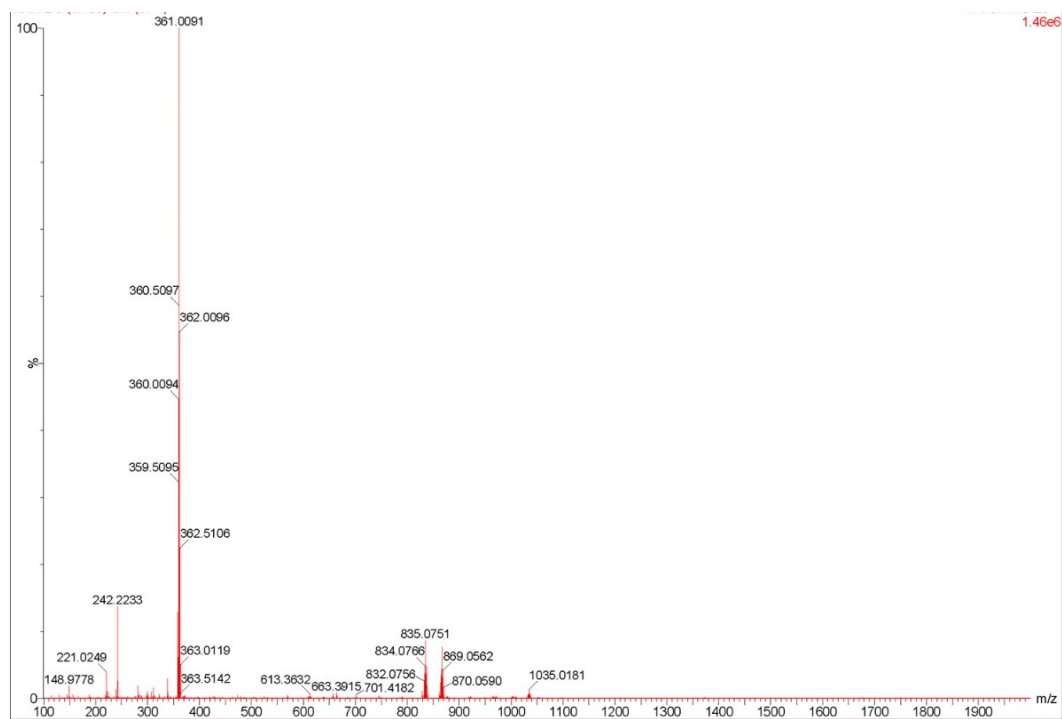**Figure S1.** ^{1}H NMR (400 MHz) spectra of (top) 4'-pyridyl-2,2':6',2''-terpyridine (PT) and (bottom) 4'-phenyl-2,2':6',2''-terpyridine (PhT) in CDCl₃.
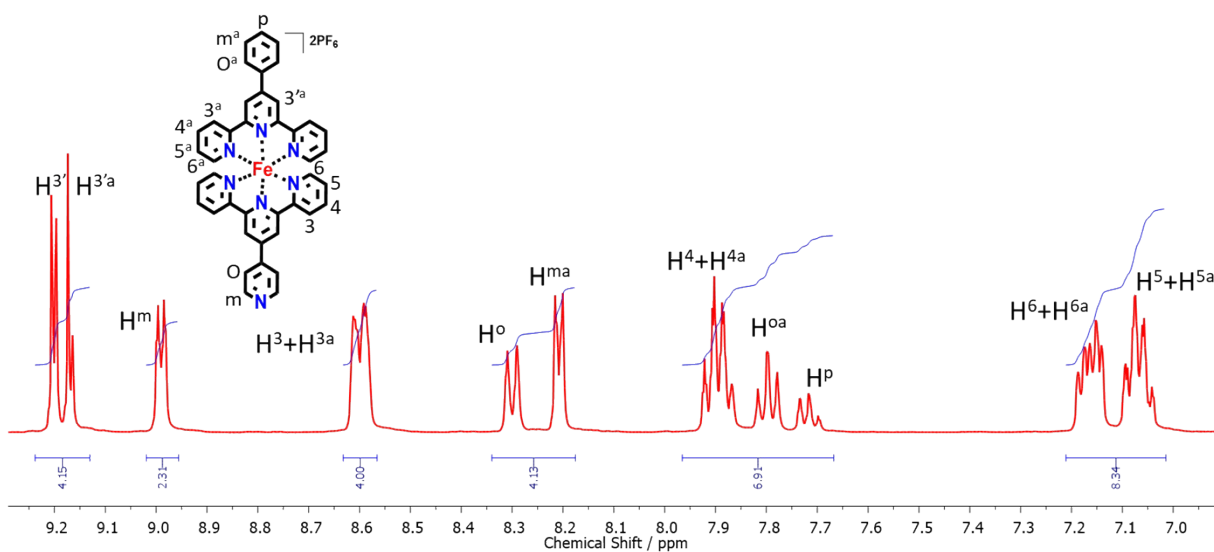
Figure S2. ^{1}H NMR (400 MHz) spectrum of **1** in DMSO-d₆.
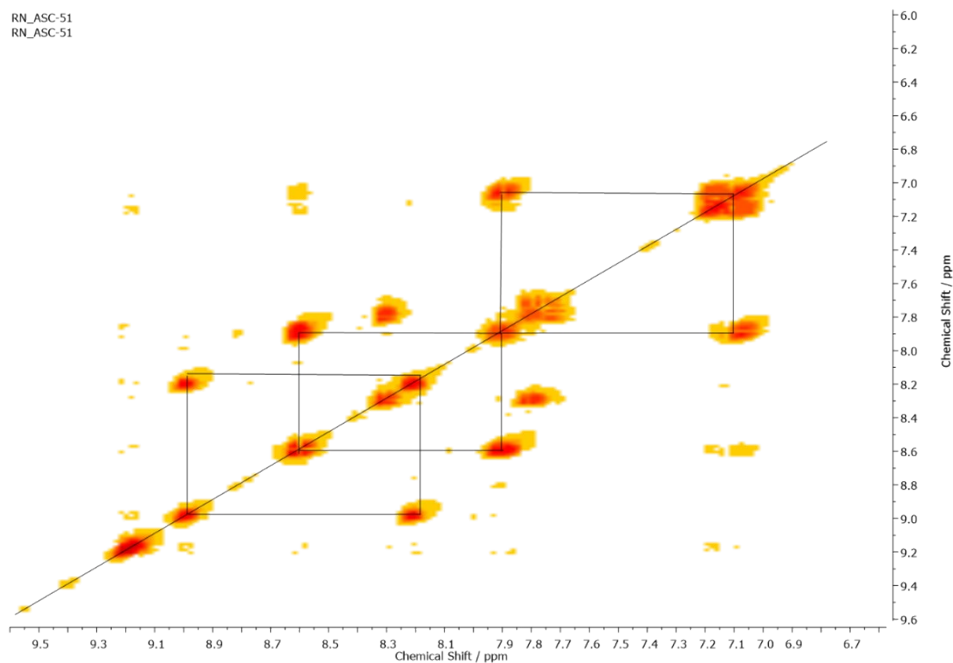
Figure S3. ^{1}H-^{1}H COSY spectrum of **1** in DMSO-d$_6$.

Figure S4. ESI-MS (+ve mode) of **1** in CH$_3$CN. Molecular ion peak correspond to [(M-(PF$_6$)$_2$)/2] + Na$^+$.
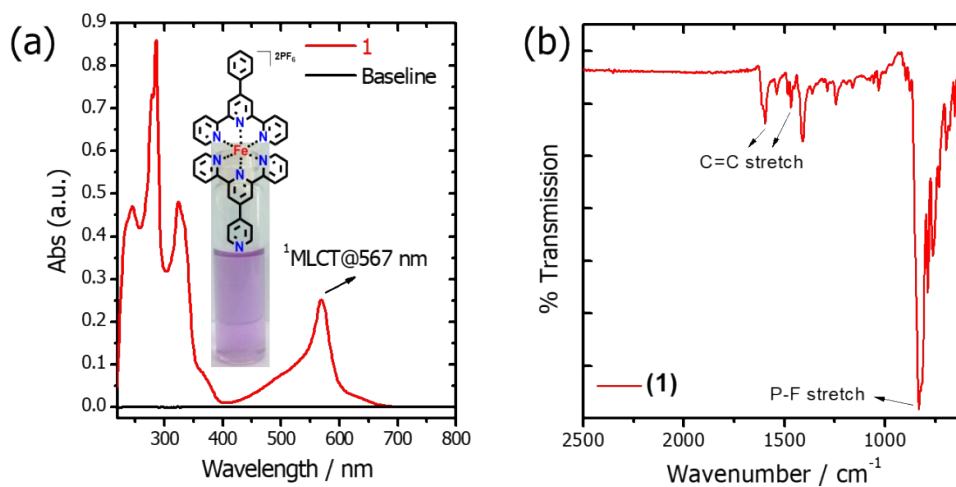
Figure S5. (a) UV-vis spectrum of **1**(10^{-5} M, CH$_3$CN); (b) ATR-IR spectrum of **1**.
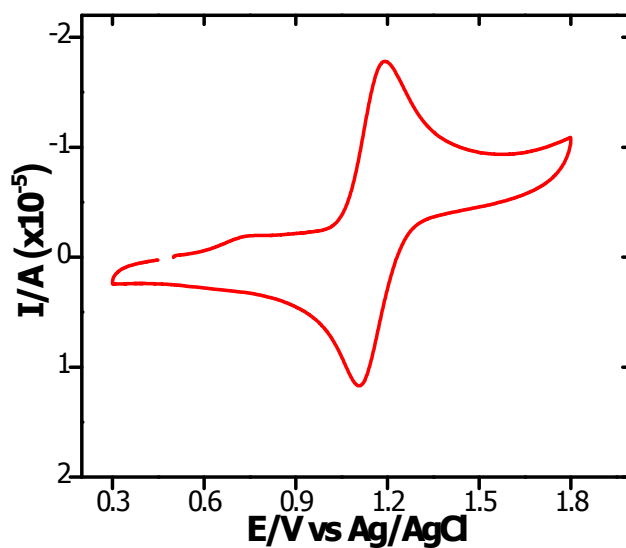
Figure S6. Cyclic voltammogram of **1** recorded at 100 mV s^{-1}. The voltammograms were recorded in dry acetonitrile (1 mM solution in 0.1 M of TBAP$_6$).

Figure S7. Photograph of **1** (10^{-5} M in CH$_3$CN) and with added analytes. It clearly depicts that only CN$^-$, F$^-$ and OH$^-$are able to change the color of **1** while other anions elicited no response.
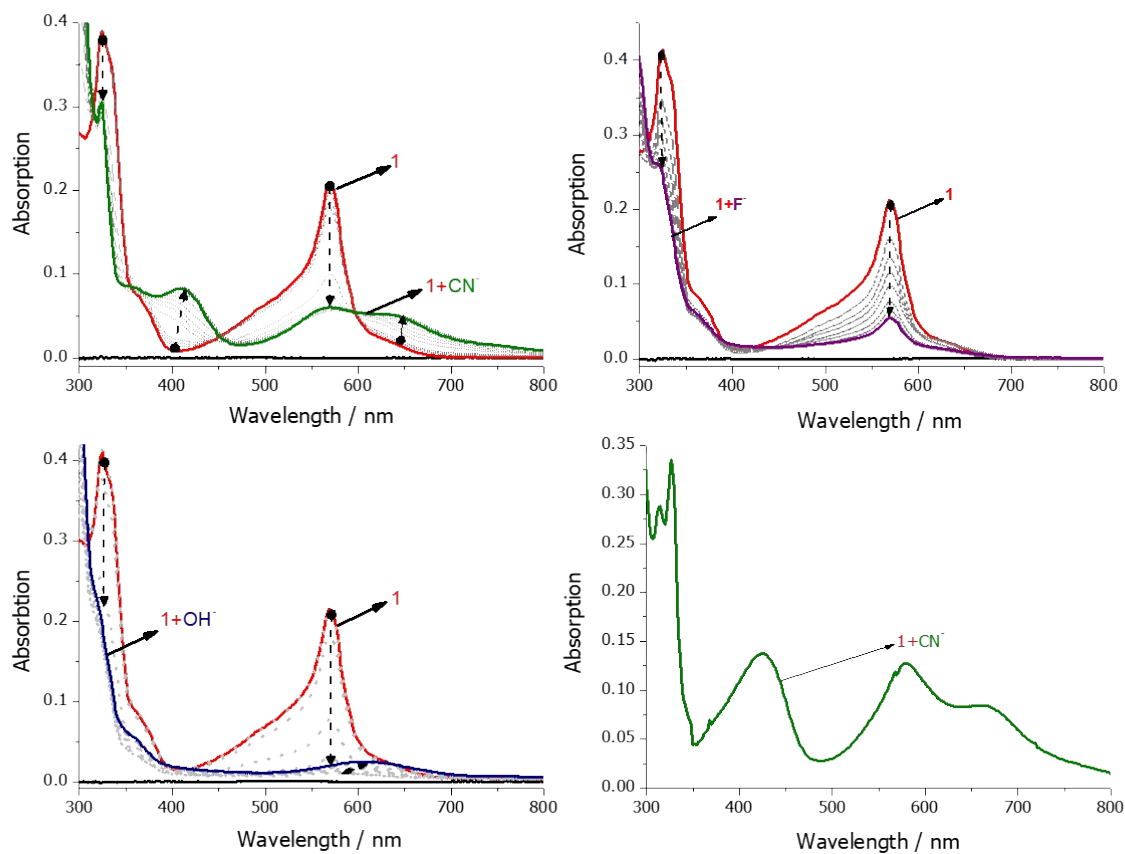
Figure S8. UV-vis spectral changes in **1** (10^{-5} M, CH$_3$CN) with the addition of ppm levels of aqueous solution of CN$^-$ (top left), F$^-$ (top right) and OH$^-$ (bottom left). UV-vis spectrum of **1**+CN$^-$ crystal dissolve in CH$_3$CN (10^{-5} M) (bottom right).
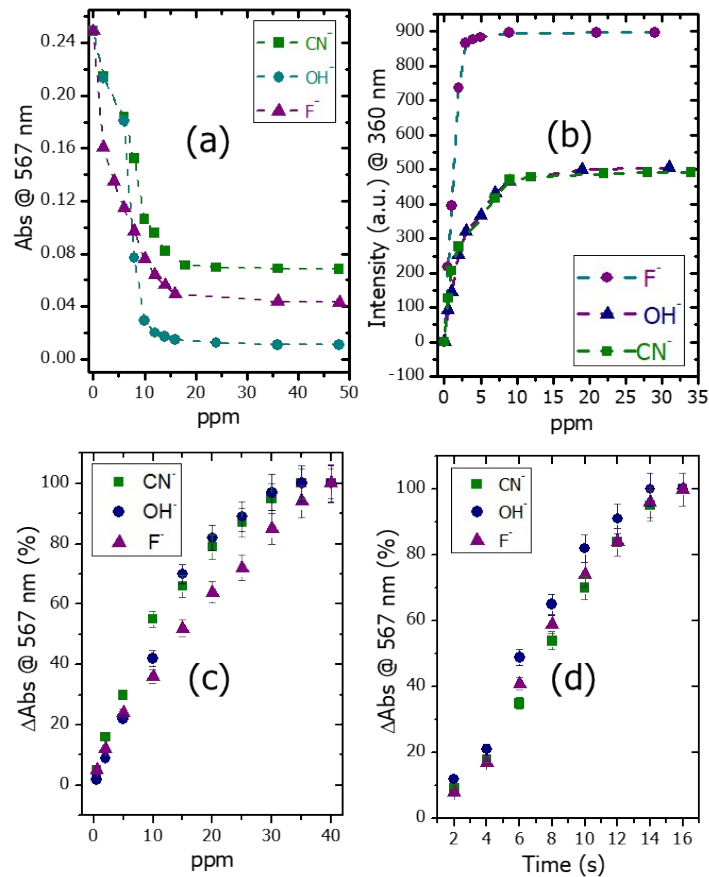
Figure S9: (a) Absorbance changes at λ_{max} = 567 nm with the addition of ppm levels of $CN^-/F^-/OH^-$. (b) Intensity changes at λ_{max} = 360 nm with the addition of ppm levels of $CN^-/F^-/OH^-$. (c) change in the absorption signal at λ_{max} = 567 nm from **1**-based sensor as a function of $CN^-/F^-/OH^-$ concentration at a fixed exposure time of 30s; (d) and as a function of time at a fixed $CN^-/F^-/OH^-$ concentration of 30 ppm.
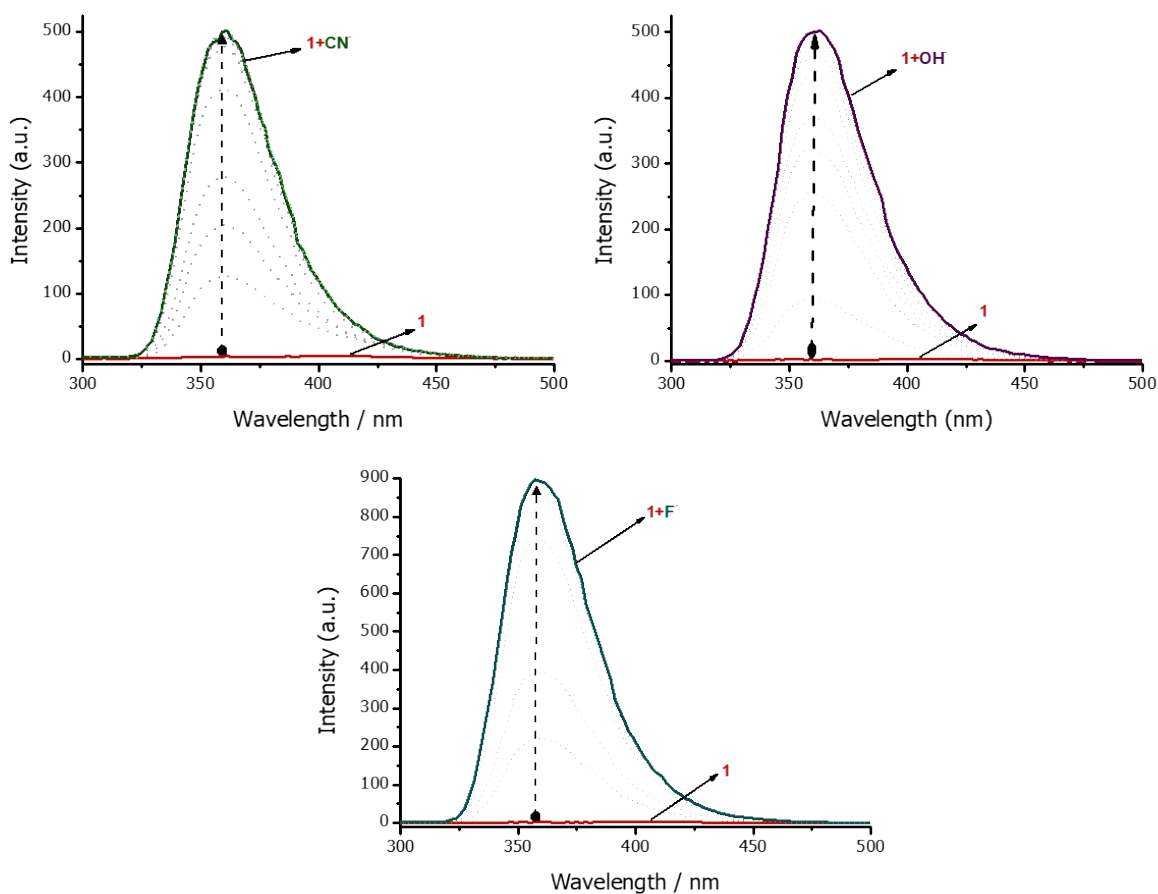
Figure S10. Changes in fluorescence intensity of **1** (10^{-5} M, CH_3CN) with the addition of ppm levels of either of CN^- (top left), OH^- (top right) and F^- (bottom) in water.

Crystallographic Information:

A crystal of appropriate size was mounted on a glass fiber and the intensity data for **1**+CN^- were collected on an Oxford Xcalibur S CCD area detector diffractometers using graphite monochromatized Mo-Kα radiation at 293(2) K. CrysAlisPro, an Agilent Technologies software package,[S4] was used for data collection and data integration for **1**+CN^-. Structure solution and refinement were carried out using the SHELXTL-PLUS software package.[S6] The non-hydrogen atoms were refined with anisotropy thermal parameters. All the hydrogen atoms were treated using appropriate riding models. The computer programme PLATON was used for analyzing the interaction and stacking distances.[S5]

Molecular structure of the complex **1**+CN¯ was determined crystallographically. Complex **1**+CN¯ crystallizes in the monoclinic system with P21 space group. The coordination geometry about iron is distorted octahedral, which is covalently bound with all the three major coordination sites of 4'-(phenyl)-terpyridine and three cyanide groups. The distances between Fe and N from the central pyridyl rings are 1.876(8) Å, which are shorter than the distances between Fe and N from the outer pyridine rings of 1.987(8) Å and 1.994(8) Å. In addition to the difference in bond lengths, the bond angles around Fe are also different and can be divided into two parts: *transoid* angles (N(1)-Fe(1)-N(3)= 161.4(4)°) and *cisoid* angles ranging from 80.6(3)° to 80.8(4)°. Since the distances and angles are not equal, a distorted octahedral geometry is apparent. The phenyl ring is not coplanar with terpyridine (tpy) ring and is tilted with respect to the tpy ring plane at an angle of 14.03º. All Fe-N and Fe-C bond distances are comparable to the values reported in the literature. The three cyanide groups are linearly attached to iron centre [N(4)-C(22)-Fe(1)= 177.1(12)°, N(5)-C(23)-Fe(1)= 177.6(12)°, N(6)-C(24)-Fe(1)= 176.3(10)°]. An interesting feature of the crystal packing in **1**+CN¯ is the infinite 1D chains resulting from the coordination of the K$^+$ ion to the cyanide groups and some waters molecules.

Table S1. Crystallographic data for **1**+CN¯.

Empirical Formula	$C_{96}H_{76}N_{24}O_{11}Fe_4K_4$
FW	2121.60
crystal system	Monoclinic
spacegroup	P21
a, Å	13.003(3)
b, Å	26.767(5)
c, Å	14.013(3)
α, deg	90.00
β, deg	103.41(3)
γ, deg	90.00
V, Å^3	4744.3(18)

Z	2
d_{calc}, g cm^{-3}	1.485
μ, mm^{-1}	0.849
T, K	293(2)
R_1all	0.1767
$R_1[I > 2\sigma(I)]$	0.0833
wR_2	0.1404
$wR_2[I > 2\sigma(I)]$	0.1023
GoF	1.001

Table S2. Selected bond lengths (Å), and Bond angles (°) for **1+CN$^-$**.

Fe(1)-N(2)	1.876(8)
Fe(1)-N(1)	1.994(8)
Fe(1)-N(3)	1.987(8)
N(1)-C(1)	1.351(12)
N(1)-C(5)	1.368(12)
N(2)-C(6)	1.343(12)
N(2)-C(10)	1.376(11)
N(3)-C(15)	1.346(12)
N(3)-C(11)	1.357(12)
N(4)-C(22)	1.145(14)
N(5)-C(23)	1.164(13)
N(6)-C(24)	1.174(13)
N(4)-K(4)[#1]	3.108(12)
N(5)-K(1)	2.798(10)
N(5)-K(4)[#1]	3.025(11)

N(5)-K(2)	3.095(11)
N(6)-K(2)	2.928(10)
C(22)-K(4)[#1]	3.279(12)
C(23)-K(4)[#1]	3.207(12)
C(23)-K(2)	3.355(13)
C(24)-K(2)	3.268(11)
Fe(1B)-N(2B)	1.879(8)
Fe(1B)-N(3B)	1.991(8)
Fe(1B)-N(1B)	1.987(9)
N(1B)-C(1B)	1.336(12)
N(1B)-C(5B)	1.362(11)
N(2B)-C(6B)	1.349(12)
N(2B)-C(10B)	1.359(11)
N(3B)-C(15B)	1.337(14)
N(3B)-C(11B)	1.368(11)
N(4B)-C(22B)	1.150(13)
N(5B)-C(23B)	1.150(13)
N(6B)-C(24B)	1.126(13)
N(4B)-K(2)	3.022(9)
N(5B)-K(3)	2.843(10)
N(5B)-K(2)	2.941(10)
Fe(1A)-N(2A)	1.901(8)
Fe(1A)-N(1A)	1.981(9)
Fe(1A)-N(3A)	1.979(9)
N(1A)-C(1A)	1.338(12)
N(1A)-C(5A)	1.366(12)
N(2A)-C(10A)	1.343(12)

N(2A)-C(6A)	1.344(12)
N(3A)-C(15A)	1.336(12)
N(3A)-C(11A)	1.365(11)
N(4A)-C(22A)	1.155(15)
N(5A)-C(23A)	1.169(12)
N(6A)-C(24A)	1.149(13)
N(4A)-K(3)	3.202(11)
N(5A)-K(2)	2.785(9)
N(5A)-K(3)	3.018(11)
N(5A)-K(1)	3.192(11)
N(6A)-K(1)	2.849(9)
C(22A)-K(3)	3.382(11)
C(23A)-K(3)	3.257(11)
C(23A)-K(1)	3.464(11)
C(24A)-K(1)	3.328(10)
Fe(1C)-N(2C)	1.892(8)
Fe(1C)-N(3C)	1.984(8)
Fe(1C)-N(1C)	1.987(9)
N(1C)-C(1C)	1.351(12)
N(1C)-C(5C)	1.373(12)
N(2C)-C(6C)	1.334(12)
N(2C)-C(10C)	1.349(12)
N(3C)-C(15C)	1.350(13)
N(3C)-C(11C)	1.358(14)
N(4C)-C(22C)	1.145(13)
N(5C)-C(23C)	1.163(12)
N(6C)-C(24C)	1.160(12)

N(4C)-K(1)#2	3.087(11)
N(5C)-K(1)#2	3.010(10)
N(5C)-K(4)	2.857(11)
K(1)-K(2)	3.985(4)
K(1)-K(4)#1	4.284(4)
K(3)-K(2)	4.229(4)
K(3)-K(4)	4.330(4)
K(4)-K(1)#2	4.284(4)
N(2)-Fe(1)-N(1)	80.6(3)
C(23)-Fe(1)-N(1)	98.4(4)
C(24)-Fe(1)-N(1)	90.5(4)
C(22)-Fe(1)-N(1)	90.6(4)
N(2)-Fe(1)-N(3)	80.8(3)
C(23)-Fe(1)-N(3)	100.2(4)
C(24)-Fe(1)-N(3)	90.2(4)
C(22)-Fe(1)-N(3)	90.8(4)
N(1)-Fe(1)-N(3)	161.4(4)
N(4)-C(22)-Fe(1)	177.1(12)
N(5)-C(23)-Fe(1)	177.6(12)
N(6)-C(24)-Fe(1)	176.3(10)
N(2B)-Fe(1B)-C(23B)	177.1(4)
N(2B)-Fe(1B)-N(3B)	80.2(4)
N(2B)-Fe(1B)-N(1B)	80.9(4)
N(1B)-Fe(1B)-N(3B)	160.8(4)
N(4B)-C(22B)-Fe(1B)	176.3(10)
N(5B)-C(23B)-Fe(1B)	173.8(12)
N(6B)-C(24B)-Fe(1B)	174.5(10)

N(2A)-Fe(1A)-C(23A)	178.7(4)
N(2A)-Fe(1A)-N(1A)	80.7(4)
N(3A)-Fe(1A)-N(1A)	161.5(4)
N(4A)-C(22A)-Fe(1A)	176.2(11)
N(5A)-C(23A)-Fe(1A)	176.9(11)
N(6A)-C(24A)-Fe(1A)	172.1(9)
N(2C)-Fe(1C)-C(23C)	177.1(4)
N(2C)-Fe(1C)-N(3C)	81.1(4)
N(2C)-Fe(1C)-N(1C)	79.5(4)
N(3C)-Fe(1C)-N(1C)	160.0(4)
N(4C)-C(22C)-Fe(1C)	175.1(12)
N(5C)-C(23C)-Fe(1C)	175.1(11)
N(6C)-C(24C)-Fe(1C)	174.0(11)
K(1)-N(5)-K(2)	84.9(3)
K(4)[#1]-N(5)-K(2)	178.5(4)
K(1)-N(5)-K(4)[#1]	94.6(3)
K(3)-N(5B)-K(2)	94.0(3)
K(2)-N(5A)-K(1)	83.3(3)
K(3)-N(5A)-K(1)	173.0(4)
K(4)-N(5C)-K(1)[#2]	93.8(3)
N(5)-K(1)-N(5C)[#1]	74.2(3)
N(6A)-K(1)-N(5C)[#1]	107.2(3)
N(6A)-K(1)-K(2)	117.6(2)
K(1)-K(2)-K(3)	97.94(8)
O(3S)-K(4)-K(3)	120.55(19)
K(1)[#2]-K(4)-K(3)	134.78(9)
K(3)-O(11S)-K(4)	95.1(4)

K(4)-O(11A)-K(3)	100.5(10)		
K(4)-O(2S)-K(3)	97.9(3)		

Table S3. Hydrogen bond parameters for **1**+CN⁻.

| D-H⋯A-X	d H⋯A Å	D D⋯A Å	θ D-H⋯A°
C(21)-H(21)⋯N (6A)[a]	2.59	3.374(14)	142
O(1S)-H(1SA)⋯N(6)	2.08	2.938(13)	160
O(1S)-H(1SB)⋯N(6C)[b]	2.09	2.890(12)	150
O(3S)-H(3SA)⋯N(6A)[b]	2.14	2.962(12)	153
O(3S)-H(3SB)⋯N(6B)	2.02	2.891(12)	168
O(5S)-H(5SA)⋯O(4S)	2.07	2.895(13)	164
O(5S)-H(5SB)⋯O(10S)[b]	2.28	2.881(12)	128
O(6S)-H(6SA)⋯O(9S)	2.54	2.823(16)	101
O(6S)-H(6SB)⋯N(4B)	2.04	2.867(14)	166
O(7S)-H(7SA)⋯N(4A)[c]	2.25	3.089(18)	168
O(7S)-H(7SB)⋯N(4)	2.28	2.944(15)	136
O(10S)-H(10A)⋯N(5B)[c]	2.41	3.066(14)	135
O(10S)-H(10B)⋯O(7S)	2.18	2.925(15)	147
O(8S)-H(8SA)⋯N(4A)[c]	2.04	2.888(15)	178
O(8S)-H(8SB)⋯N(4)	2.57	2.983(17)	111
O(8S)-H(8SB)⋯O(11S)[c]	2.29	2.724(19)	112
O(9S)-H(9SA)⋯O(6S)	2.14	2.823(16)	137
O(9S)-H(9SB)⋯N(5C)	2.16	2.987(16)	164

symmetry equivalents: (a) x,y,1+z; (b) 1-x,1/2+y,1-z; (c)1-x,-1/2+y,1-z.
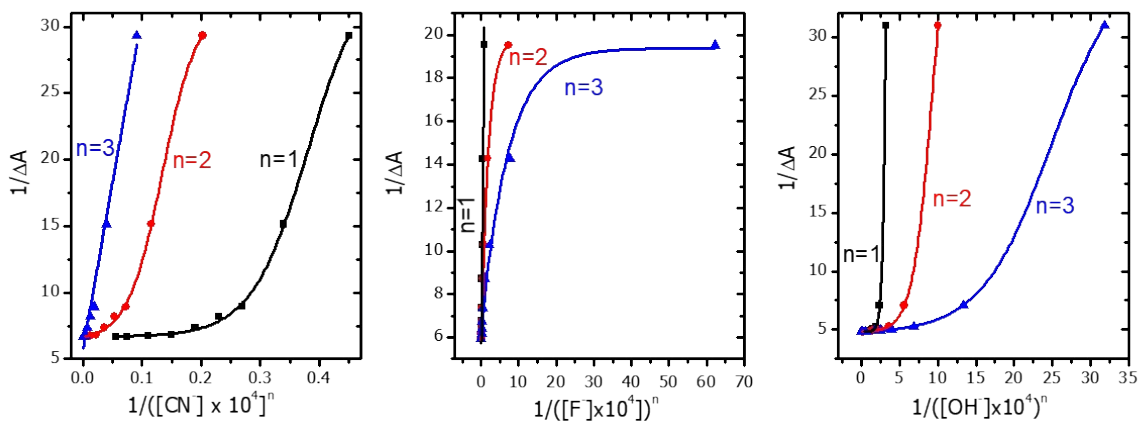
Figure S11. Benesi-Hildebrand plot for **1**+CN⁻ (left), **1**+F⁻ (middle) and **1**+OH⁻ (right) (R^2 = ~0.98-0.99) from UV-vis data, respectively.
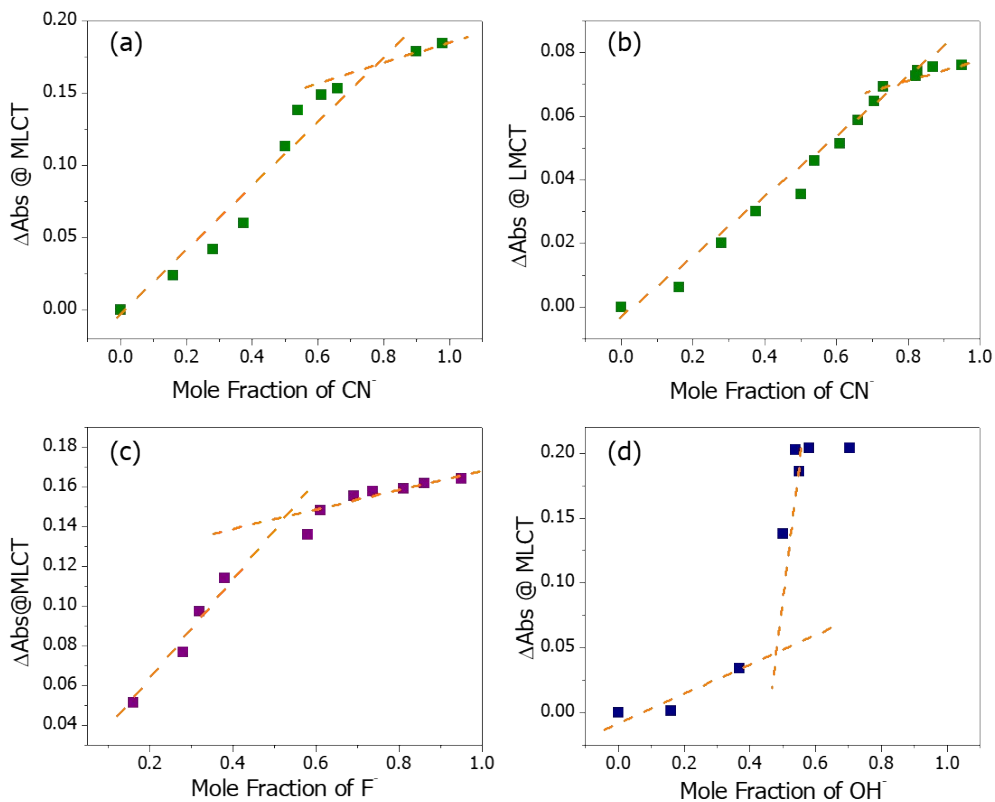
Figure S12. Determination of binding ratio of 1+anion interaction using Job's method of continued variation of mole fraction (a) 1+CN⁻ using MLCT band (λ = 567 nm); (b) 1+CN⁻ using LMCT band (λ = 412 nm); (c) 1+F⁻ using MLCT band (λ = 567 nm); (d) 1+CN⁻ using MLCT band (λ = 567 nm).
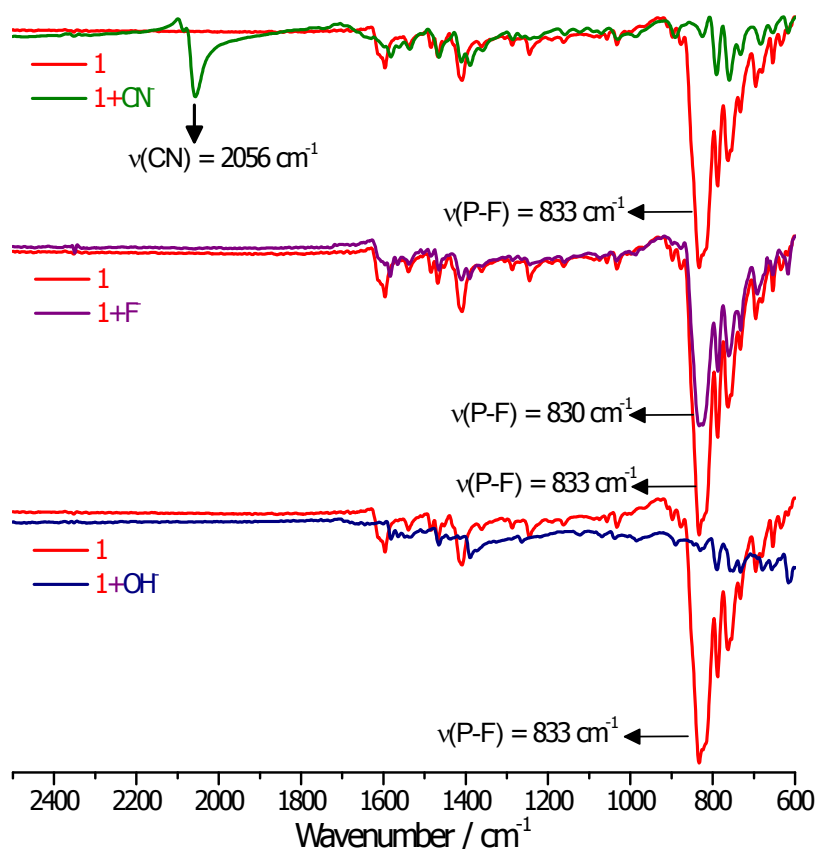
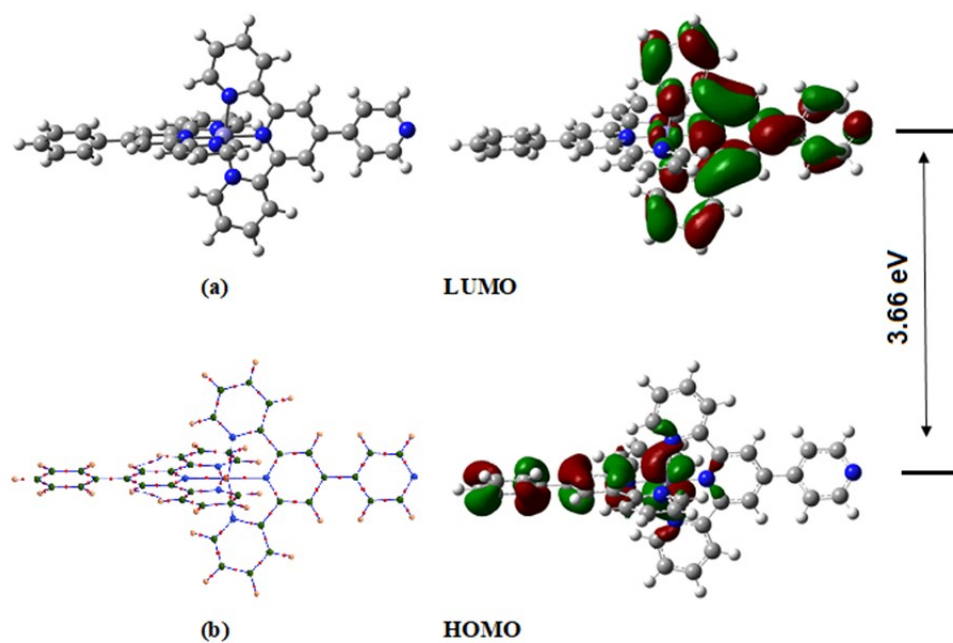

Figure S13. ATR-IR spectra of **1** and **1**+anions.

**Table S4.** Analytical results for the detection of CN⁻/F⁻/OH⁻ in spiked tap water samples.

S. No.	CN⁻ added (ppm)	CN⁻ found (ppm)	F⁻ added (ppm)	F⁻ found (ppm)	OH⁻ added (ppm)	OH⁻ found (ppm)
1	5	4.8	5	5.6	5	6.1
2	15	16.7	15	14.4	15	16.8
3	30	31.4	30	28.1	30	32.4
4	60	58.6	60	58.9	60	63.2

5	150	147.2	150	146.2	150	154.8

(a)   LUMO

3.66 eV

(b)   HOMO

Figure S14. Left panel: (a) The optimized molecular structure of **1** and (b) Molecular graph obtained using Atoms-in-Molecules calculations. Right panel: HOMO, LUMO and LUMO+1 frontier orbitals isosurfaces and their energy gaps.

LUMO   LUMO   LUMO

HOMO   HOMO   HOMO

HOMO-1

1   **1** + OH⁻   **1** + F⁻
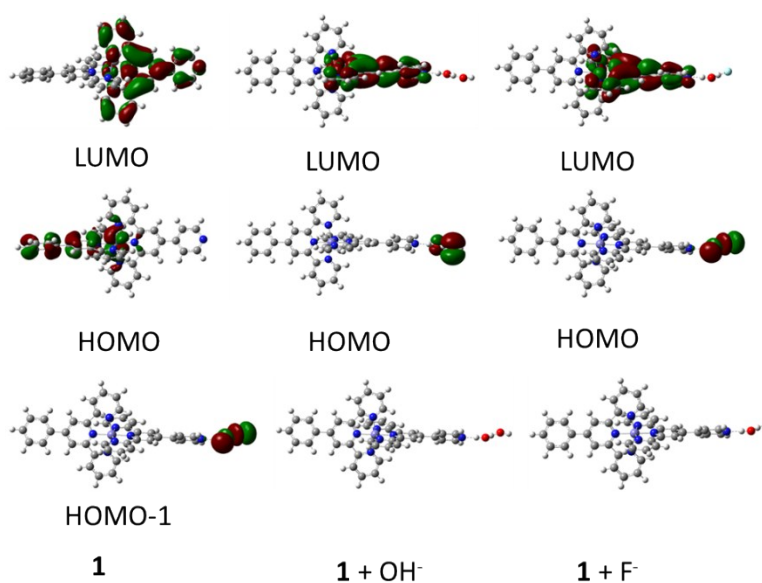
Figure S15. Selected orbital transitions for 1, 1+OH⁻(H$_2$O) and 1+F⁻(H$_2$O) obtained by TD-DFT calculations using solvent parameters of acetonitrile.

References:

S1. D. D. Perrin and W. L. F. Armarego, *Purification of Laboratory Chemicals*, 3. Aufl., Oxford. Pergamon Press, 1988.

S2. V. Singh, P. C. Mondal, J. Y. Lakshmanan, M. Zharnikov and T. Gupta, *Analyst*, 2012, **137**, 3216-3219.

S3. A. Winter, A. M. van den Berg, R. Hoogenboom, G. Kickelbick and U. S. Schubert, *Synthesis*, 2006, **17**, 2873-2878.

S4. G.M. Sheldrick, *Acta Crystallogr., Sect. A: Found. Crystallogr.*, 2007, **64**, 112.

S5. (*a*) G.M. Sheldrick, SHELX-97 Programme for Refinement of Crystal Structures, University of Gottingen, Gottingen, Germany, 1997; (*b*) A.L. Spek, PLATON, *Acta Crystallogr., Sect. A: Found. Crystallogr.*, 1990, **46A**, C34.]

S6. J.-D. Chai and M. Head-Gordon, *Phys. Chem. Chem. Phys.*, 2008, **10**, 6615-6620.

S7. S. Miertuš, E. Scrocco and J. Tomasi, *Chem. Phys.*, 1981, **55**, 117-129.

S8. M. Cossi, V. Barone, R. Cammi and J. Tomasi, *Chem. Phys. Lett.*, 1996, **255**, 327-335.

S9. Gaussian 09, Revision D.01, M. J. Frisch, G. W. Trucks, H. B. Schlegel, G. E. Scuseria, M. A. Robb, J. R. Cheeseman, G. Scalmani, V. Barone, B. Mennucci, G. A. Petersson, H. Nakatsuji, M. Caricato, X. Li, H. P. Hratchian, A. F. Izmaylov, J. Bloino, G. Zheng, J. L. Sonnenberg, M. Hada, M. Ehara, K. Toyota, R. Fukuda, J. Hasegawa, M. Ishida, T. Nakajima, Y. Honda, O. Kitao, H. Nakai, T. Vreven, J. A. Montgomery, Jr., J. E. Peralta, F. Ogliaro, M. Bearpark, J. J. Heyd, E. Brothers, K. N. Kudin, V. N. Staroverov, R. Kobayashi, J. Normand, K. Raghavachari, A. Rendell, J. C. Burant, S. S. Iyengar, J. Tomasi, M. Cossi, N. Rega, J. M. Millam, M. Klene, J. E. Knox, J. B. Cross, V. Bakken, C. Adamo, J. Jaramillo, R. Gomperts, R. E. Stratmann, O. Yazyev, A. J. Austin, R. Cammi, C. Pomelli, J. W. Ochterski, R. L. Martin, K. Morokuma, V. G. Zakrzewski, G.

A. Voth, P. Salvador, J. J. Dannenberg, S. Dapprich, A. D. Daniels, Ö. Farkas, J. B. Foresman, J. V. Ortiz, J. Cioslowski, and D. J. Fox, Gaussian, Inc., Wallingford CT, 2009.

S10. G. Henkelman, A. Arnaldsson, H. Jónsson, Comput. Mater. Sci, 2006, **36**, 354-360.